Replica Ornstein-Zernike self-consistent theory for mixtures in random pores

G. Pellicane and C. Caccamo
Dipartimento di Fisica, Università di Messina and Istituto Nazionale per la Fisica della Materia (INFM), Messina, Italy

D. S. Wilson and L. L. Lee*
School of Chemical Engineering and Materials Science, University of Oklahoma, Norman, Oklahoma 73019, USA
(Received 4 December 2003; published 4 June 2004)

We present a self-consistent integral equation theory for a binary liquid in equilibrium with a disordered medium, based on the formalism of the replica Ornstein-Zernike (ROZ) equations. Specifically, we derive direct formulas for the chemical potentials and the zero-separation theorems (the latter provide a connection between the chemical potentials and the fluid cavity distribution functions). Next we solve a modified-Verlet closure to ROZ equations, which has built-in parameters that can be adjusted to satisfy the zero-separation theorems. The degree of thermodynamic consistency of the theory is also kept under control. We model the binary fluid in random pores as a symmetrical binary mixture of nonadditive hard spheres in a disordered hard-sphere matrix and consider two different values of the nonadditivity parameter and of the quenched matrix packing fraction, at different mixture concentrations. We compare the theoretical structural properties as obtained through the present approach with Percus-Yevick and Martinov-Sarkisov integral equation theories, and assess both structural and thermodynamic properties by performing canonical standard and biased grand canonical Monte Carlo simulations. Our theory appears superior to the other integral equation schemes here examined and provides reliable estimates of the chemical potentials. This feature should be useful in studying the fluid phase behavior of model adsorbates in random pores in general.

DOI: 10.1103/PhysRevE.69.061202 PACS number(s): 61.20.Gy, 61.20.Ja, 64.70.Ja

I. INTRODUCTION

Phase changes of liquids inside porous media are of both scientific and technological interest. Porous materials, such as activated carbon, silica gels, zeolites, pillared clay and more recently, aerogels, aminosilicates, aluminophosphate, carbon nanotubes, Vycor glass, microporous BN, and starburst dendrimers have been extensively used in industry for adsorption, dehumidification, catalysis, gas separation [1], and gas storage [2,3]. Many of these systems have an amorphous structure, that is, they consist of microsized pores that are irregularly distributed throughout the material. For example, aerogels have a cobweblike structure that is made up of cross interconnecting inorganic/organic colloidal-like particles or polymeric chains with high porosity $(75-99\%)$ [4]. When fluids invade the interior of such materials, the confinement in narrow dimensions deeply changes the *bulk* phase behavior, as has been well documented [5]. Only a few theoretical studies have looked into binary fluid mixtures in random pores [6]. The simplest model for these systems, exhibiting a stable phase separation, is exemplified by the nonadditive hard sphere mixture (NAHSM).

In this paper we employ both integral equations (IE) of the replica type [7] and computer simulations in order to characterize the structure and the thermodynamics of NAHSM under confinement. The effect of confinement is assured by the presence of a disordered, rigid matrix of hard spheres. The study of this basic model should help in understanding both the effects of nonadditivity and of porosity on phase properties in general.

In our approach, we improve the performance of the replica-Ornstein-Zernike (OZ) integral equations by requiring both conformity to the zero-separation theorems and a partial thermodynamic consistency. This combined methodology has been applied and tested in a number of previous studies: on pure hard spheres in bulk [8] and in pores [9], additive [10] and nonadditive [11] hard sphere mixtures in bulk, Lennard-Jones molecules [12], and diatomic hard dumbbells [13]. In all cases, close agreement was obtained between IE and simulation. The essence of such an approach is the use of the zero separation theorems (ZST) [14], in addition to the usual thermodynamic consistencies [15]. The values of correlation functions at zero distance (when two particles coincide) obey certain exact conditions that tie them to the thermodynamic properties of the system under study, such as the chemical potentials and the isothermal compressibility. This is, in a way, similar to the contact value theorem for hard-core systems [16]. The difference between ZST and thermodynamic consistencies is in the "local" (specific values of the correlation functions are required at some distances) nature of the former versus the "global" (almost everywhere) nature of the latter. Both types of consistencies reinforce the "accuracy" of the integral equation formulation based on the replica OZ equations. For the aforementioned reason, we specifically develop zero-separation theorems of model mixtures in random pores, and we adapt them to our particular model system. Next, we solve a modified-Verlet closure [17] to the replica OZ equations which has built-in, adjustable parameters and we tune them so as to satisfy the zero-separation theorems (ZSEP closure). We refer to the present implementation of ZSEP as a self-consistent closure only to the satisfaction of zero-separation theorems; on the other hand, its degree of thermodynamic consistency is

*Corresponding author. Email address: lle@ou.edu

monitored as well on the basis of the Gibbs-Duhem relation. We also solve the replica OZ equations under the Percus-Yevick (PY, [18]) and Martinov-Sarkisov (MS, [19]) integral equation closures. In order to test the accuracy of the theoretical calculations, we have carried out Monte Carlo (MC, [20]) simulations in three different ensembles: the *NVT* [*NVT*, (standard constant number of particles) $\times$ (constant volume) $\times$ constant temperature)] canonical ensemble, the grand canonical ensemble [21], and the cavity-biased grand canonical ensemble [22]. A number of conditions are investigated, representing different nonadditivities ($\Delta=0.2,0.4$), matrix porosities ($\rho_0=0.18,0.3$), mixture densities ($0.18 \leqslant \rho^* \leqslant 0.35$), and compositions of the binary mixture ($\chi=0.1,0.3,0.5$).

In Sec. II, we present the theoretical framework and the simulation procedures. In Sec. III, we show the results for the radial distribution functions, the chemical potentials and a case-study for the liquid-liquid equilibrium. Finally, we give some concluding remarks and perspectives in Sec. IV.

II. THE MODEL AND THE METHODS

A. Model

We consider a binary mixture of nonadditive hard-sphere particles:

$$\boldsymbol{V}_{ij}(\boldsymbol{r}) = \begin{cases} \infty & r \leqslant \sigma_{ij} \\ 0 & r > \sigma_{ij} \end{cases}, \tag{1}$$

where σ_{ij} are the diameters of interaction among species i and j, $\sigma_{12}=(1+\Delta)[(\sigma_{11}+\sigma_{22})/2] > \sigma_{11}=\sigma_{22}$ and Δ is the nonadditive parameter. The fluid mixture is confined in a matrix of random, nonoverlapping hard-sphere particles of diameter σ_0. Throughout the paper we will use the notation $\sigma_1=\sigma_{11}$ and $\sigma_2=\sigma_{22}$. Within this model for the fluid mixture, a positive nonadditivity in the cross interaction between the two species favors homocoordination in comparison to heterocoordination. As a consequence of the extra repulsion from unlike interactions, nonadditive hard-sphere mixtures are expected to separate, at sufficiently high density, into two distinct phases. We consider this model because it is the simplest mixture possible to exhibit a thermodynamically stable liquid-liquid transition. In all the calculations we assume that the size of the two species is equal to the diameter of the matrix sphere, i.e., $\sigma_{11}=\sigma_{22}=\sigma_0$, briefly stated we consider symmetrical mixtures. Then, we study the effect of increasing nonadditivity from 20% to 40% ($\Delta=0.2,0.4$) on the structure and on the thermodynamics of the system.

B. Theory

The formalism of the replica OZ (ROZ) equations was derived for the first time for pure fluids by Madden-Glandt and Given-Stell, and recently extended to binary liquids by Paschinger and Kahl (see Ref. [7] and references therein). These equations describe the structure of a binary liquid inside a disordered medium and are formally derived after a partial quenching of one of the components and in the limiting case for $s=0$ of a fully equilibrated $(2s+1)$-component system, where $s=s_1+s_2$ is the number of identical copies of the liquid mixture species (the replicas); thus, within this formalism, the mixture confined into the rigid matrix is depicted as a semiquenched system (partly quenched and partly annealed). The label 0 indicates the matrix species, 1 and 2 the liquid mixture species, 3 and 4 any replica of 1 and 2, respectively. In the following, we adopt the matrix notation of Ref. [7] for the correlation functions $h_{ij}(r)$and $c_{ij}(r)$, and we suppress the argument r in order to improve readability; the replica OZ equations are so written as ("**T**" denotes the transpose of a vector and $\otimes$ is a convolution):

$$h_{00} = c_{00} + \rho_0 c_{00} \otimes h_{00},$$

$$\mathbf{h}_{01} = \mathbf{c}_{01} + \mathbf{h}_{01} \otimes \rho_0 \mathbf{c}_{00} + \rho_1 \mathbf{h}_{11} \otimes \mathbf{c}_{01} - \rho_1 \mathbf{h}_{12} \otimes \mathbf{c}_{01},$$

$$\mathbf{h}_{11} = \mathbf{c}_{11} + \mathbf{h}_{01} \otimes \rho_0 \mathbf{c}_{01}^{\mathrm{T}} + \rho_1 \mathbf{h}_{11} \otimes \mathbf{c}_{11} - \rho_1 \mathbf{h}_{12} \otimes \mathbf{c}_{12},$$

$$\mathbf{h}_{12} = \mathbf{c}_{12} + \mathbf{h}_{01} \otimes \rho_0 \mathbf{c}_{01}^{\mathrm{T}} + \rho_1 \mathbf{h}_{12} \otimes \mathbf{c}_{11} + \rho_1 \mathbf{h}_{12} \otimes \mathbf{c}_{12} \mathrm{b} - 2\rho_1 \mathbf{h}_{12} \otimes \mathbf{c}_{12}, \tag{2}$$

where

$$\rho_1 = \begin{pmatrix} \boldsymbol{\rho}_1 & \mathbf{0} \\ \mathbf{0} & \boldsymbol{\rho}_2 \end{pmatrix}, \quad \mathbf{h}_{01} = \begin{pmatrix} \mathbf{h}_{01} \\ \mathbf{h}_{02} \end{pmatrix}, \quad \mathbf{c}_{01} = \begin{pmatrix} \mathbf{c}_{01} \\ \mathbf{c}_{02} \end{pmatrix}, \tag{3}$$

$$\mathbf{h}_{11} = \begin{pmatrix} \mathbf{h}_{11} & \mathbf{h}_{12} \\ \mathbf{h}_{12} & \mathbf{h}_{22} \end{pmatrix}, \quad \mathbf{c}_{11} = \begin{pmatrix} \mathbf{c}_{11} & \mathbf{c}_{12} \\ \mathbf{c}_{12} & \mathbf{c}_{22} \end{pmatrix},$$

$$\mathbf{h}_{12} = \begin{pmatrix} \mathbf{h}_{13} & \mathbf{h}_{14} \\ \mathbf{h}_{14} & \mathbf{h}_{24} \end{pmatrix}, \quad \mathbf{c}_{12} = \begin{pmatrix} \mathbf{c}_{13} & \mathbf{c}_{14} \\ \mathbf{c}_{14} & \mathbf{c}_{24} \end{pmatrix}. \tag{4}$$

The total number of the coupled ROZ equations is eight, though the first one is the bulk OZ equation for the matrix particles. The ROZ equations are solved under different closures, namely, the modified-Verlet closure [17]:

$$B_{ij}(r) = -\frac{\zeta_{ij}}{2} \gamma_{ij}^{*2} \left(1 - \phi_{ij} + \frac{\phi_{ij}}{1 + \alpha_{ij} \gamma_{ij}^*} \right), \tag{5}$$

where $B_{ij}(r)$and $\gamma_{ij}^*(r)$ are the bridge and the renormalized indirect correlation functions, respectively; the renormalization of the indirect correlation function is achieved by adding a soft-Weeks Chandler Andersen (WCA) potential [23] to the γ_{ij} function, $\gamma_{ij}^*(r)=\gamma_{ij}(r)+\frac{1}{2}\rho f_{ij}(r)$, where $f_{ij}(r)$ is the Mayer factor of the repulsive WCA 6:3 potential. The introduction of this term circumvents the discontinuities in the bridge functions when combined with the closure; we slightly modified the indirect correlation function by setting the pseudotemperature in the Mayer factor $\approx 10^4$. The twenty-four adjustable parameters ζ_{ij}, ϕ_{ij}, and α_{ij} (three parameters for each of the eight ROZ equations) appear to be excessive; then, we drastically reduce this number by letting them assume "reasonable" values according to the following criteria: we always set $\alpha_{ij}=1$ and we use two different sets of parameters for equimolar and asymmetric concentrations, respectively. The choice to fix the set α_{ij} to unity is related to the functional form of the modified Verlet closure (5). In fact, the

partial derivative of the bridge function with respect to the α_{ij} is still a function of α_{ij}, in contrast the two partial derivatives with respect to the ζ_{ij} and ϕ_{ij} do not depend on ζ_{ij} and ϕ_{ij}, respectively.

Thus, independent variations of ζ_{ij} and ϕ_{ij}, will affect the bridge functions in a plain way, and we might expect that such a linear behavior would be beneficial for speeding up the numerical search of consistent bridge functions. For the equimolar concentrations we set: $\zeta_1=\zeta_{11}^{\mathrm{SYM}}=\zeta_{22}^{\mathrm{SYM}}$, $\zeta_2=\phi_2=\zeta_{12}^{\mathrm{SYM}}=\zeta_{14}^{\mathrm{SYM}}=\phi_{12}^{\mathrm{SYM}}=\phi_{14}^{\mathrm{SYM}}$, $\zeta_3=\zeta_{10}^{\mathrm{SYM}}=\zeta_{20}^{\mathrm{SYM}}$, $\zeta_4=\zeta_{33}^{\mathrm{SYM}}=\zeta_{44}^{\mathrm{SYM}}$, $\phi_1=\phi_{11}^{\mathrm{SYM}}=\phi_{22}^{\mathrm{SYM}}$, $\phi_3=\phi_{10}^{\mathrm{SYM}}=\phi_{20}^{\mathrm{SYM}}$, $\phi_4=\phi_{33}^{\mathrm{SYM}}=\phi_{44}^{\mathrm{SYM}}$; as far as the asymmetric concentrations are concerned, we fix the values of the ζ_{ij} to the symmetrical concentration ones, $\zeta_{ij}=\zeta_{ij}^{\mathrm{SYM}}$, and we allow all the ϕ_{ij} to vary under the constraint $\phi_{12}=\phi_{14}$. We note that the bridge functions are strongly affected by variations of the ζ_{ij} at all distances (and this obviously holds also at $r=0$), because this set appears as a multiplying coefficient to them [see Eq. (5)]; then, the choice to fix the ζ_{ij} to the symmetrical counterparts hinges upon the following arguments: we surmise that the variability of the correlation functions nearby $r=0$ originates mainly from the total packing fraction and only slightly from the exact value of the concentration. Though we may expect this conjecture to be reasonable for symmetrical species, a different approach would be desirable when asymmetric species (in size) are present in the mixture; in fact, in this latter case the height of the correlation functions is likely to vary considerably when concentration is different from the equimolar one. In both cases, we end up with seven parameters to be determined by enforcing self-consistency theorems. We adopt zero separation theorems, which relate the cavity functions values at zero distance to the proper expression for the chemical potentials. In a previous paper, one of us reported the formulas of the chemical potentials for bulk mixtures [11,24]; here we derive these formulas for the system representing the matrix and the mutually noninteracting s_1, s_2 copies (replicas) of the fluid species. We introduce the following short-hand notation:

$$\rho_k \int [ij] = \rho_k \int d\mathbf{r} \left(\ln y_{ij} - h_{ij} + \frac{1}{2} h_{ij}\gamma_{ij} + h_{ij}B_{ij} - S_{ij} \right), \tag{6}$$

where $\gamma_{ij}(r)$ and $S_{ij}(r)$ are, respectively, the indirect correlation functions and the Star functions introduced earlier [24], and ρ_k is the number density of species k. Thus, the monomer chemical potentials are easily written as (all chemical potentials are configurational quantities, in excess of the ideal part):

$$\beta\mu_0 = \rho_0 \int [00] + \mathbf{s}\rho_1 \int [01] + \mathbf{s}\rho_2 \int [02],$$

$$\beta\mu_1 = \rho_0 \int [10] + \rho_1 \int [11] + (\mathbf{s}_1 - \mathbf{1})\rho_3 \int [13] + \rho_2 \int [12] + (\mathbf{s}_2 - \mathbf{1})\rho_4 \int [14],$$

$$\beta\mu_2 = \rho_0 \int [20] + \rho_2 \int [22] + (\mathbf{s}_2 - \mathbf{1})\rho_4 \int [24] + \rho_1 \int [21] + (\mathbf{s}_1 - \mathbf{1})\rho_3 \int [23],$$

$$\beta\mu_3 = \rho_0 \int [30] + \rho_3 \int [33] + (\mathbf{s}_1 - \mathbf{1})\rho_{3'} \int [33'] + \rho_4 \int [34] + (\mathbf{s}_2 - \mathbf{1})\rho_{4'} \int [34'],$$

$$\beta\mu_4 = \rho_0 \int [40] + \rho_4 \int [44] + (\mathbf{s}_2 - \mathbf{1})\rho_{4'} \int [44'] + \rho_3 \int [43] + (\mathbf{s}_1 - \mathbf{1})\rho_{3'} \int [43'], \tag{7}$$

where $3'$ and $4'$ are replicas of 1 and 2 other than 3 and 4, respectively, $\beta=1/k_{\mathrm{B}}T$, T is the absolute temperature and k_{B} is the Boltzmann constant.

Now, the reversible works of insertion of *dimers* made up from pairs of species $1+1, 2+2, 1+2, 1+0, 2+0, 1+3, 2+4$ as they merge into zero bond length (at infinite dilution in the mixture) are the chemical potentials for *dimers* of the corresponding pairs at coincidence ($r=0$) (Note: $1+2$ denotes the dimer species formed from species 1 and species 2):

$$\beta\mu_{1+1} = \rho_0 \int [1+1,0] + \rho_1 \int [1+1,1] + (\mathbf{s}_1 - \mathbf{1})\rho_3 \int [1+1,3] + \rho_2 \int [1+1,2] + (\mathbf{s}_2 - \mathbf{1})\rho_4 \int [1+1,4]$$

$$\beta\mu_{2+2} = \rho_0 \int [2+2,0] + \rho_2 \int [2+2,2] + (\mathbf{s}_2 - \mathbf{1})\rho_4 \int [2+2,4] + \rho_1 \int [2+2,1] + (\mathbf{s}_1 - \mathbf{1})\rho_3 \int [2+2,3]$$

$$\beta\mu_{1+0} = \rho_0 \int [1+0,0] + \rho_1 \int [1+0,1] + (\mathbf{s}_1 - \mathbf{1})\rho_3 \int [1+0,3] + \rho_2 \int [1+0,2] + (\mathbf{s}_2 - \mathbf{1})\rho_4 \int [1+0,4]$$

$$\beta\mu_{2+0} = \rho_0 \int [2+0,0] + \rho_2 \int [2+0,2] + (\mathbf{s}_2 - \mathbf{1})\rho_4 \int [2+0,4] + \rho_1 \int [2+0,1] + (\mathbf{s}_1 - \mathbf{1})\rho_3 \int [2+0,3]$$

$$\beta\mu_{1+2} = \rho_0 \int [1+2,0] + \rho_1 \int [1+2,1] + (\mathbf{s}_1 - \mathbf{1})\rho_3 \int [1+2,3] + \rho_2 \int [1+2,2] + (\mathbf{s}_2 - \mathbf{1})\rho_4 \int [1+2,4]$$

$$\beta\mu_{1+3} = \rho_0 \int [1+3,0] + \rho_1 \int [1+3,1] + \rho_3 \int [1+3,3] + \rho_2 \int [1+3,2] + \rho_4 \int [1+3,4] + (\mathbf{s}_1 - \mathbf{2})\rho_{3'} \int [1+3,3'] + (\mathbf{s}_2 - \mathbf{2})\rho_{4'} \int [1+4,4']$$

$$\beta\mu_{2+4} = \rho_0 \int [2+4,0] + \rho_2 \int [2+4,2] + \rho_4 \int [2+\mathbf{4},4] + \rho_1 \int [2+4,1] + \rho_3 \int [2+\mathbf{4},3] + (\mathbf{s}_2 - \mathbf{2})\rho_{4'} \int [2+\mathbf{4},4'] + (\mathbf{s}_1 - \mathbf{2})\rho_{3'} \int [2+\mathbf{4},3']. \quad (8)$$

These formulas are general and are applicable to any type of interaction pair potential. Now we shall specialize the above relations to the case of nonadditive hard-sphere mixtures in the hard-sphere matrix and we shall also formulate the zero-separation theorems. For the 11 cavity functions

$$\ln y_{11}(0) = 2\beta\mu_1 - \beta\mu_{1+1} = \beta\mu_1. \quad (9)$$

Thus, we have (upon taking the limit $s_1 \to 0, s_2 \to 0$:)

$$\ln y_{11}(0) = \rho_0 \int [10] + \rho_1 \int [11] - \rho_3 \int [13] + \rho_2 \int [12] - \rho_4 \int [14]. \quad (10)$$

In a similar way, we can build up the zero-separation theorems for the other cavity functions:

$$\ln y_{22}(0) = \rho_0 \int [20] + \rho_2 \int [22] - \rho_4 \int [24] + \rho_1 \int [21] - \rho_3 \int [23]$$

$$\ln y_{13}(0) = \rho_0 \int [10]$$

$$\ln y_{24}(0) = \rho_0 \int [20] \quad (11)$$

We note that the coincidence value of the mixture-replica cavity functions depends only on the matrix-fluid correlations, similarly to the pure case [9]. The case of $\ln y_{10}(0), \ln y_{20}(0)$, and $\ln y_{12}(0)$ is a bit more complicated and we have to distinguish between different possibilities. In fact, though the treatment of zero-separation theorems between the crossed species of the real system is based on an additive rule similar to Eq. (9), a number of different simplifications between the terms appearing in the chemical potentials (8), depending on the mutual size of particles, may occur. It is then straightforward to write for the unlike cavity functions:

$$\ln y_{12}(0) = \rho_0 \int [20] + \rho_1 \int [11] + \rho_2 \int [22] - \rho_2 \int [24] - \rho_1 \int [23], \quad \sigma_1 \geqslant \sigma_2$$

$$\ln y_{12}(0) = \rho_0 \int [20] + \rho_1 \int [11] + \rho_2 \int [22] - \rho_1 \int [13] - \rho_2 \int [14], \quad \sigma_1 \leqslant \sigma_2 \quad (12)$$

while for the particle-matrix cavity functions:

$$\ln y_{10}(0) = \rho_0 \int [00] - \rho_1 \int [13] - \rho_2 \int [14] + \rho_1 \int [01] + \rho_2 \int [02], \quad \sigma_1 > \sigma_0$$

$$\ln y_{10}(0) = \rho_0 \int [01] + \rho_1 \int [11] - \rho_1 \int [13] + \rho_2 \int [12] - \rho_2 \int [14], \quad \sigma_1 \leqslant \sigma_0$$

$$\ln y_{20}(0) = \rho_0 \int [00] - \rho_2 \int [24] - \rho_1 \int [23] + \rho_2 \int [02] + \rho_1 \int [01], \quad \sigma_2 > \sigma_0$$

$$\ln y_{20}(0) = \rho_0 \int [02] + \rho_2 \int [22] - \rho_2 \int [24] + \rho_1 \int [12] - \rho_1 \int [23], \quad \sigma_2 \leqslant \sigma_0 \quad (13)$$

Thus, the closure Eq. (5) to the ROZ equations is solved numerically under the constraint determined by the seven Eqs. (10)–(13). We also checked the ability of this closure to guarantee internal thermodynamic consistency. Unfortunately, the virial equation of state for the quenched-annealed system is not straightforwardly related to structural functions as for bulk mixtures [25]; in fact for hard-core interactions:

$$\beta P = \rho_0 \left(\frac{\partial \beta P}{\partial \rho_0} \right)_{VT\mu_1\mu_2} + \sum_i \rho_i - \frac{2\Pi}{3} \left[\rho_0^2 \sigma_{00}^3 \lim_{s \to 0} \frac{dg_{00}(\sigma_{00}; s)}{ds} + \sum_{i=1,2} \rho_i^2 \sigma_{ii}^3 g_{ii}(\sigma_{ii}) + 2 \sum_{i=1,2} \rho_0 \rho_i \sigma_{0i}^3 g_{0i}(\sigma_{0i}) + 2\rho_1 \rho_2 \sigma_{12}^3 g_{12}(\sigma_{12}) \right], \quad (14)$$

where the first term is the infinitesimal change of the virial pressure with respect to the matrix density at constant values of volume, temperature, and chemical potentials of the two species, and $\lim_{s \to 0} [dg_{00}(\sigma_{00}; s)/ds]$ is the infinitesimal change

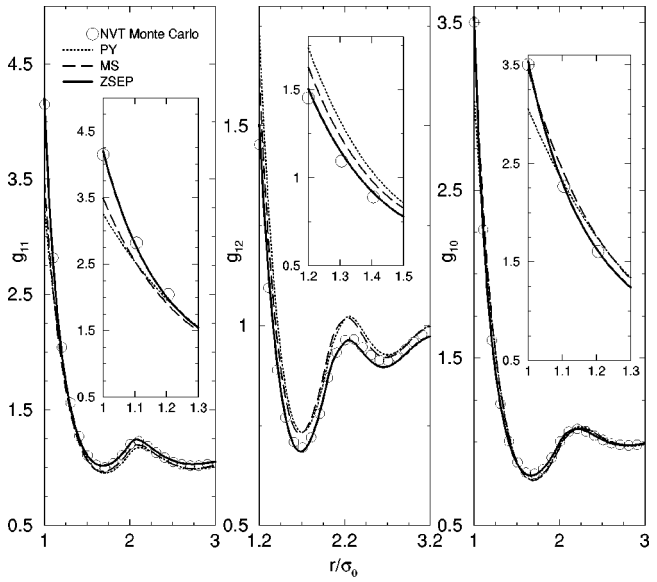

FIG. 1. Radial distribution functions for the mixture at $\Delta=0.2, \rho_0=0.3, \chi=0.5$. Full line, ZSEP; long-dashed line, MS; dotted line, PY; open circles, NVT Monte Carlo simulation.

of the matrix-matrix radial distribution function in the replicated system with respect to the number of replicas, in the limit of the quenched-annealed system. Both quantities should be evaluated numerically, and in particular the first one implies the calculation of the product of two numerical derivatives, as a standard mathematical manipulation of thermodynamic derivatives shows:

$$\left(\frac{\partial \beta P}{\partial \rho_0}\right)_{VT\mu_1\mu_2} = \left(\frac{\partial \beta P}{\partial \rho_0}\right)_{VTN_1N_2} - \sum_{i=1,2}\left[\left(\frac{\partial \beta P}{\partial \mu_i}\right)_{VTN_1N_2}\left(\frac{\partial \mu_i}{\partial \rho_0}\right)_{VTN_1N_2}\right]. \tag{15}$$

Thus, we resort to a different strategy in order to monitor the thermodynamic consistency of the theory; in particular, we use the Gibbs-Duhem relation [12],

$$\left(\frac{\partial \beta P}{\partial \rho}\right)_{VTN\rho_0} = \sum_{j=1,2}\chi_j\left[\sum_{i=1,2}\rho_i\left(\frac{\partial \beta\mu_i}{\partial \rho_j}\right)_{VTN_{k\neq j}\rho_0}\right] = [\rho k_B T\chi_T]^{-1} = 1 - \sum_{i,j=1,2}\chi_i\chi_j\rho\tilde{c}_{ij}^{c}(0), \tag{16}$$

where the chemical potentials of the two species are differentiated numerically in order to obtain the inverse of the isothermal compressibility and $\tilde{c}_{ij}^{c}(0)$ are the Fourier transforms at zero wave vector of the connected part of the direct correlation functions, within the ROZ formalism. We recall that direct correlation functions may be distinguished, on the basis of a diagrammatical analysis, by a connected c_c and a blocked part c_b, respectively, so that $c=c_c+c_b$ [7].

The ROZ equations are also solved under the PY [18] closure:

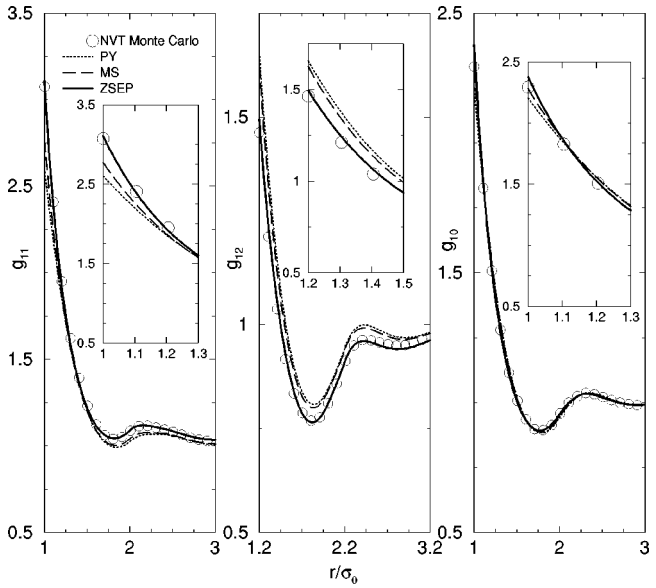

FIG. 2. Radial distribution functions for the mixture at $\Delta=0.2, \rho_0=0.1, \chi=0.5$. See FIG. 1 for the meaning of the symbols.

$$c_{ij}(r) = [\exp^{-\beta V_{ij}(r)} - 1][1 + \gamma_{ij}(r)] \tag{17}$$

and the MS [19] closure:

$$c_{ij}(r) = \exp^{-\beta V_{ij}(r) - 1 + \sqrt{1+0.5\gamma_{ij}(r)}}. \tag{18}$$

We solve numerically the different closures to the ROZ equations with a Picard method and adopt a standard mixing procedure for the direct correlation function in order to ensure convergence; normally, 1024 grid points with grid interval 0.01 σ_0 are used but we also checked the stability of the solution with higher grids of 2048, 4096 points for some thermodynamic state points. Zero-separation theorems and the thermodynamic constraint (16) are enforced in the frame-

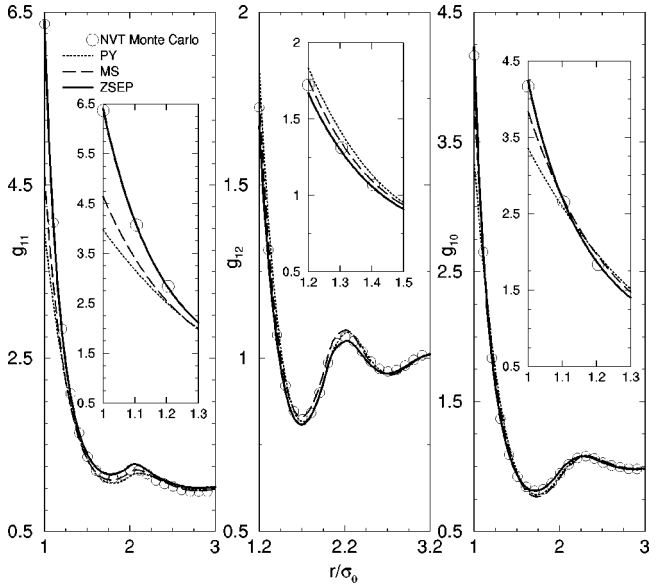

FIG. 3. Radial distribution functions for the mixture at $\Delta=0.2, \rho_0=0.3, \chi=0.1$. See FIG. 1 for the meaning of the symbols.

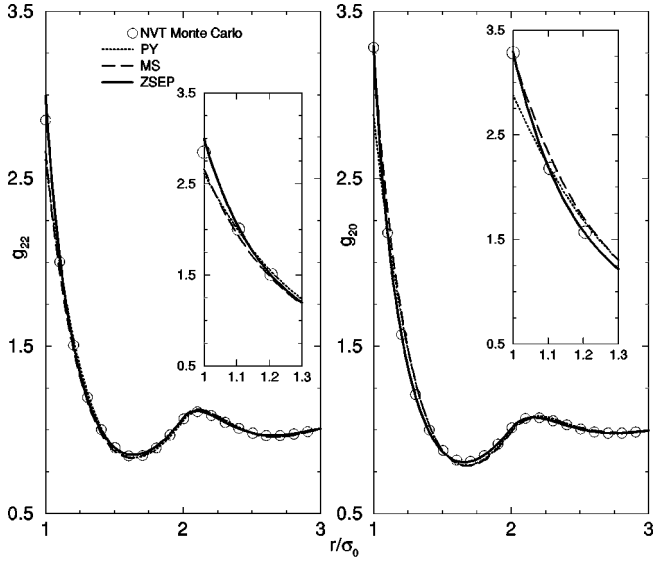

FIG. 4. Radial distribution functions for the mixture at $\Delta=0.2, \rho_0=0.3, \chi=0.1$. See FIG. 1 for the meaning of the symbols.

work of the modified-Verlet closure (ZSEP) with a tolerance of 1%. The numerical procedure adopted to fulfill self-consistency according to Eqs. (10)–(13) turns out to be a smart one, notwithstanding the apparent difficulty of dealing with a system of seven equations in seven unknown variables. In fact, each equation turns out to be a functional strongly dependent just on the correlation functions with the same label of the cavity function y_{ij}. Thus, the overall system is slightly coupled and we can obtain a rapid guess of the solution by applying simultaneously an indipendent Newton-Raphson search procedure to each of the seven Eqs. (10)–(13); to such a purpose, one of the variational parameters appearing in the bridge functions B_{ij} [see Eq. (5)] is used for each zero-separation equation, and the procedure is

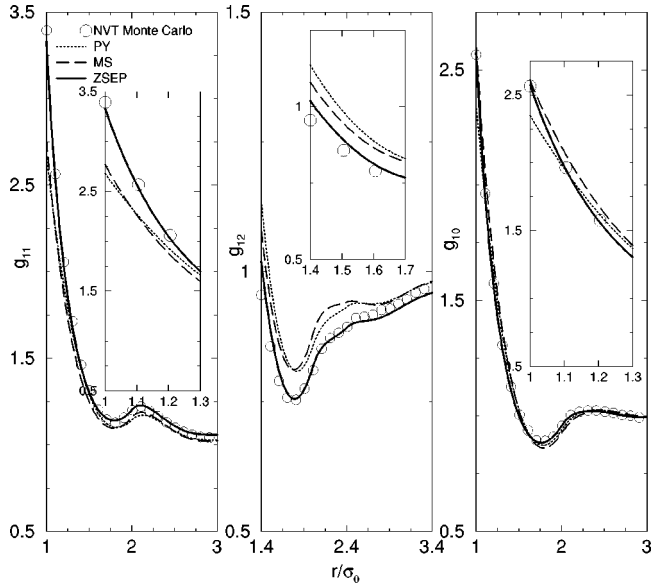

FIG. 5. Radial distribution functions for the mixture at $\Delta=0.4, \rho_0=0.3, \chi=0.5$. See FIG. 1 for the meaning of the symbols.

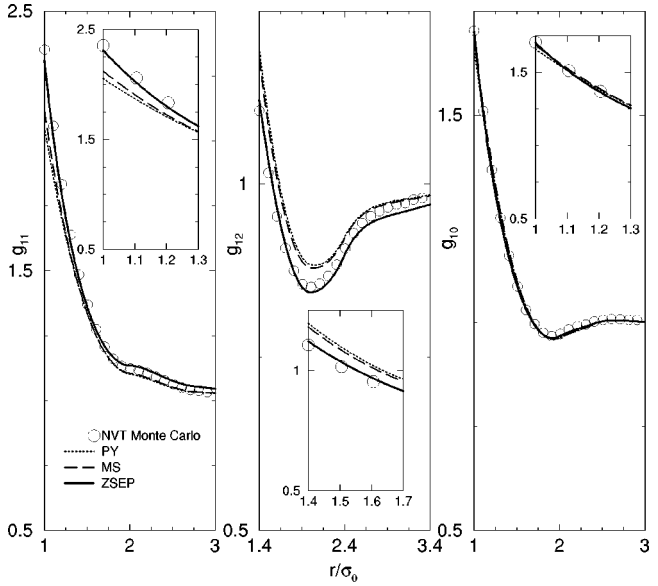

FIG. 6. Radial distribution functions for the mixture at $\Delta=0.4, \rho_0=0.1, \chi=0.5$. See FIG. 1 for the meaning of the symbols.

iterated a few cycles up to convergence. This approach is mantained essentially unaltered also when thermodynamic consistency is imposed according to Eq. (16); in this case, however, the previous cycle (denoted as ZST cycle) is completed with a refinement cycle (TC or thermodynamic consistent cycle) on an additional parameter so to satify Eq. (16). We choose ζ_1 as a variational parameter for the ZST cycle because we noticed by numerical inspection that Eq. (16) is particularly sensible to variations of it. The sequence of independent ZST and TC cycles is then iterated until convergence.

C. Simulation

We have performed Monte Carlo [20] simulations with three different simulation algorithms: the grand canonical (T,V,μ_1,μ_2) ensemble (GCMC, [21]), the cavity-biased grand canonical (CB-GCMC, [22]) ensemble and the standard *NVT* canonical ensemble [20]. The GCMC simulation is used in order to sample different matrix realizations and fluid mixture particle configurations. Simulations in order to gen-

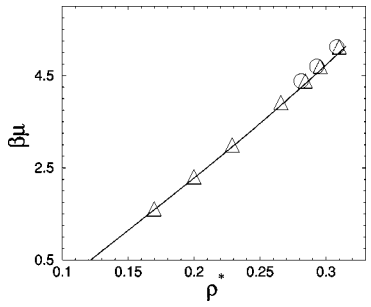

FIG. 7. Chemical potential vs total mixture density at $\Delta=0.2, \rho_0=0.2, \chi=0.5$. Triangles, grand canonical Monte Carlo simulation; circles, cavity-biased grand canonical Monte Carlo simulation; full line, ZSEP.

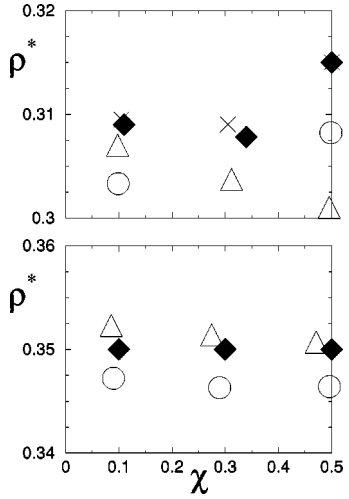

FIG. 8. Total mixture density vs particle concentration at fixed chemical potentials. $\Delta=0.2$. Triangles, grand canonical Monte Carlo simulation; open circles, cavity-biased grand canonical Monte Carlo simulation; diamonds, ZSEP; crosses, ZSEP with thermodynamic consistency.

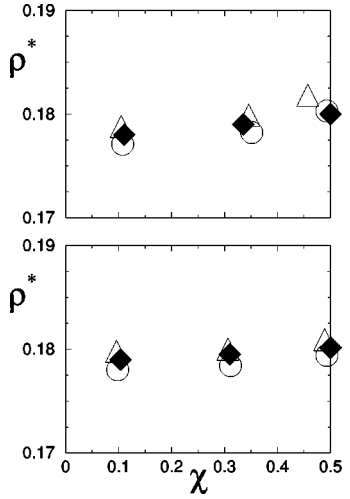

FIG. 9. Total mixture density versus particle concentration at fixed chemical potentials. $\Delta=0.4$. See Fig. 7 for the meaning of the symbols.

erate matrix realizations at the chosen mean density are performed in the GCMC ensemble as well.Three types of particles moves (displacement, creation, or destruction of a particle) were performed randomly with equal probability inside a cubic box with cubic periodic boundaries; typically, averages are collected over 30 matrix realizations and for each realization not less than 20 000–30 000 trial moves per particle are generated. Matrix realizations are generated by recording the configuration of the system every 50 000 trial moves per particle.

We also increase the efficiency of the importance sampling by performing simulations in the CB-GCMC ensemble; within this method, the acceptance probability of a molecular configuration is biased so as to favor insertions of new particles into existing cavities in the box, instead of at randomly selected points only. In particular, insertion and deletion attempts are accepted with probabilities:

$$P_i = \min\left(1, VP_c^N(\mathbf{r}^{\mathrm{N}})\frac{\exp\{\beta\mu + \beta[V(\mathbf{r}^{\mathrm{N}}) - V(\mathbf{r}^{\mathrm{N+1}})]\}}{\Lambda^3(N+1)}\right),$$

$$P_d = \min\left(1, N\Lambda^3\frac{\exp\{-\beta\mu + \beta[V(\mathbf{r}^{\mathrm{N}}) - V(\mathbf{r}^{\mathrm{N-1}})]\}}{V\,P_c^{N-1}(\mathbf{r}^{\mathrm{N-1}})}\right), \tag{19}$$

where $P_c^N(\mathbf{r}^{\mathrm{N}})$is the configuration-dependent probability of finding a cavity of diameter σ_c or larger, provided the system consists of N particles, and Λ is the de Broglie thermal wavelength. We estimated $P_c^N(\mathbf{r}^{\mathrm{N}})$ by implementing a cavity search using a finite grid. We always used a box of side length approximately equal to $13.5\sigma_0$ and a uniform grid of 100^3 points; the grid size is chosen so as to be computationally manageable while generating a negligible error in the limiting distribution of the Markov chain, since deletions can occur at any point in the box but insertions are restricted just to the grid points.

Finally, we perform *NVT* simulations from previously equilibrated GCMC simulations, in order to evaluate the radial distribution functions.

III. RESULTS AND DISCUSSION

We begin to assess the structural properties as predicted by integral equation closures against standard *NVT* simulations. In Figs. 1 and 2, from the left to right panels, we report

TABLE I. Consistency parameters and percentage thermodynamic inconsistency (%TI) for different mixtures at the equimolar concentration. In the top of the table $\rho_0=(N_0/V)\sigma_0^3, \rho^*=[(N_1+N_2)/V]\sigma_0^3, \chi=N_1(N_1+N_2)$.

Δ	ρ_0	ρ^*	χ	%TI	ζ_1	ζ_2	ζ_3	ζ_4	ϕ_1	ϕ_3	ϕ_4
0.2	0.3	0.31	0.5	1.8	0.6868	1.0111	0.77995	0.8325	0.9553	0.9853	1.1792
0.2	0.3	0.315	0.5	0.5	0.6868	1.0111	0.77995	0.8325	0.9553	0.9848	1.1722
0.2	0.1	0.35	0.5	2.5	0.6726	1.1113	0.8565	1.74695	0.9407	1.0591	2.3981
0.4	0.3	0.18	0.5	2.8	0.5637	1.0687	0.7406	0.7361	0.9198	1.0276	1.2120
0.4	0.1	0.18	0.5	0.7	0.6032	1.6598	1.1328	-0.1468	0.9394	1.5889	0.02915

TABLE II. Consistency parameters and percentage thermodynamic inconsistency (%TU) for different mixtures. See Table I for the meaning of the symbols.

Δ	ρ_0	ρ^*	χ	%**TI**	ϕ_{11}	ϕ_{12}	ϕ_{22}	ϕ_{01}	ϕ_{02}	ϕ_{33}	ϕ_{44}
0.2	0.3	0.3078	0.34	8.6	0.9566	1.0077	0.9530	0.9931	0.9763	1.0905	1.2428
0.2	0.3	0.3090	0.305	0.8 (ζ_1=0.5208)	0.9237	1.0092	0.9530	0.9941	0.9758	1.08446	1.2443
0.2	0.3	0.309–0.31	0.1–0.11	13	0.9560	0.9988	0.9500	1.010	0.9679	0.9922	1.2789
0.2	0.3	0.3095	0.105	0.3 (ζ_1=0.1961)	0.7045	1.005	0.9495	1.0087	0.9684	1.0051	1.2776
0.2	0.1	0.35	0.3	6.1	0.9427	1.10045	0.9315	1.1004	1.0352	1.9334	2.7364
0.2	0.1	0.35	0.1	4.7	0.9291	1.07895	0.8929	1.1664	0.9702	1.4872	2.7578
0.4	0.3	0.179	0.335	2.9	0.9223	1.0592	0.9098	1.0584	0.9969	1.1145	1.3092
0.4	0.3	0.178	0.1105	4.8	0.9322	1.0360	0.8957	1.1124	0.9616	0.9833	1.3565
0.4	0.1	0.1795	0.310	2.9	0.95505	1.5906	0.92335	1.7837	1.42965	3.9580	−3.1866
0.4	0.1	0.179	0.104	1.5	0.9710	1.4072	0.8856	2.0898	1.2515	8.5566	−3.7338

radial distribution functions for the particle 1-particle 1, particle 1-particle 2 and particle 1-matrix short-range correlations at a equimolar composition.

It appears that for a moderate nonadditivity and for two different matrix porosities, ZSEP gives rise to the best performances, quantitatively describing the simulation profiles for all the correlations. Both PY and MS closures manifest quantitative inaccuracies, especially at short range, and it is interesting to note that confinement into a random matrix induces a moderate worsening of their performances with respect to the bulk [26]. On the other hand, ZSEP overall good performances maintain unaltered also at an asymmetric concentration as high as 10% (see Fig. 3), with a slight shift up of both the more dilute species like correlations at longer distances and of the cross correlation at distances close to contact; however, ZSEP seems to capture the correct phase and oscillations, in agreement with the other integral equation schemes here considered. Moreover, as shown in Fig. 4, also the particle 2-particle 2 and particle 2-matrix correlations are better described by ZSEP.

We also monitor in Fig. 5 the effect of increasing nonadditivity, i.e., increasing the tendency of particles to homocoordination. While ZSEP shows a slight tendency to overestimate and underestimate the like-like and the crossed correlations at longer distances, respectively, it remains definitely the most reliable integral equation closure among the ones here considered. These performances by ZSEP have been checked also at a lower degree of matrix porosity, as reported in Fig. 6. We have chosen to plot all the radial distribution functions in a narrow range (extending to approximately three matrix diamaters) in order to show evidence on the comparison between ZSEP and the other integral equation closures considered. All the radial distribution functions oscillate around 1 when longer distances are visualized, thus confirming that the states explored fall in the stable region of the thermodynamic plane. The unusual behavior shown by the cross structural functions, and in particular the marked depth of the first coordination shell, is derived from the spatial correlations due to the presence of the matrix particles.

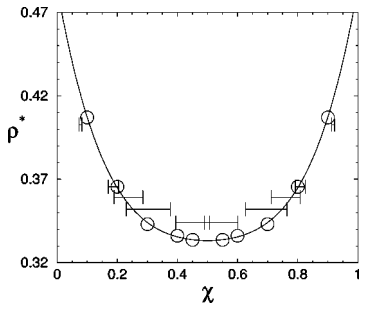

FIG. 10. Liquid-liquid phase coexistence boundary in the total mixture density-particle concentration plane for $\Delta=0.2, \rho_0=0.2$. Error bars, grand canonical Monte Carlo simulation; open circles, ZSEP; full line, curve fitting ZSEP points.

After considering structure, we turn our attention to thermodynamics and, in particular, to the ability of the theory to give reliable estimates of the chemical potential, that is a primary ingredient for the determination of the liquid-liquid phase separation envelopes.

As it appears in Fig. 7, where the calculations are performed at fixed equimolar concentration, ZSEP is able to reproduce accurately simulation results up to the mixture densities close to the region of immiscibility in the phase diagram, with a discrepancy never exceeding 2–3%.

This result is confirmed by adopting a different strategy for the assessment in Figs. 8 and 9: we use as initiation for simulations the theoretical chemical potentials and try to look at the simulation mean total mixture densities and the mean particle concentrations in comparison with the theoretical values. Again, at the worst case reported in the upper panel of Fig. 8, i.e., at the higher matrix density and at the lower mixture nonadditivity considered in this work, the percentage discrepancy with simulation was inferior to 3%. In the attempt to reduce this error of theory in comparison with simulation results, we also monitor the effect of imposing the thermodynamic constraint of Eq. (16) just for the case $\Delta=0.2, \rho_0=0.3$. To this aim, we use as an additional variational parameter the quantity ζ_1 and it emerges that decreasing the degree of thermodynamic inconsistency by ZSEP from about 10% to less than 1% brings a slight change in the calculated chemical potentials (see upper panel of Fig. 8). For this reason, we have not tried to enforce systematically the internal

thermodynamic consistency of Eq. (16) for all the cases considered in this paper. However, as documented in Tables I and II, ZSEP is not found to be thermodynamically inconsistent in a significant way, with a percentage discrepancy (%TI) which on the average is of the order of 3–4% and at the worst cases never exceeds 10–15%.

Finally, we calculate the liquid-liquid coexistence lines for the worst case (as for the comparison with simulation data) reported in the upper panel of Fig. 8 and assess ZSEP predictions with Cavity-Biased Monte Carlo simulations. Note that our conditions of simulation are similar to those of Sierra and Duda [6] who, on the other hand, performed simulations in the semigrand canonical ensemble [20]. Theoretical coexistence lines reported in Fig. 10 are calculated by equating the chemical potentials of the two species (second and third equations of Eq. (7), respectively), at different concentrations. After performing such a match, we were able to establish the lower consolute critical point, with an error of $\sim 3\%$, as compared to the simulation results. This is in conformity with the previous observation on the accuracy of the calculated chemical potentials. As far as a comparison with the bulk performances of modified Verlet closures is concerned [11], we note that we have not tried to systematically achieve thermodynamic consistency, as for instance between the virial and the compressibility equation, or between the two sides of the Gibbs-Duhem equation; this achievement is probably at the origin of the even better predictions obtained for bulk mixtures [11]. However, as far as the virial equation of state is concerned for the confined system, the possibility to use Eq. (14) is currently prevented by the absence of an efficient computational procedure to calculate the derivative of the matrix-matrix radial distribution function in the replicated system with respect to the number of replicas.

IV. CONCLUSIONS

We have demonstrated that the formalism of replica Ornstein-Zernike equations, coupled with a flexible closure satisfying zero-separation theorems, turn out able to satisfactorily reproduce the relevant structural and thermodynamic properties of nonadditive hard sphere mixtures in random pores. In particular, confinement of the NAHSM inside a porous matrix determines a worsening of PY and MS predictions of the radial distribution contact values in comparison to the bulk performances [26], with inaccuracies ranging from about 10% to nearly 20%. On the other hand, ZSEP predictions are only slightly affected by increasing of matrix density from $\rho_0=0.1$ to $\rho_0=0.3$, showing an overall discrepancy in comparison to the simulation never exceeding 2–3%. It is worth noting that we have not extensively constrained ZSEP to fulfil also thermodynamic consistency: in that case, even a better improvement should be expected on the basis of previous work upon integral equation theories [8–15]. Though the NAHSM infused into a disordered matrix of hard spheres represent a basic model, our approach, hinging on the enforcement of the validity of zero-separation theorems, can be easily generalized in the framework of a more realistic model of mixtures in random pores.

Microporous and mesoporous materials are widely used in the industry as active reservoirs for fluids, e.g., in demixing processes. On the other hand, the design of several processes involving adsorbates into amorphous materials is largely empirical at the present time, with little scientific basis. Thus, a reliable description of liquid-liquid equilibria from a modellistic point of view, as the one achieved in the present study, is of fundamental interest.

It is also worthwhile to remark that a computational approach based on replica-OZ equations is sensibly more advantageous than simulation: in fact, on a typical workstation, we verified that the computational load necessary to numerically solve the theory for the structure is about three orders of magnitude less than a fully equilibrated simulation (as the typical one performed in the present study).

Recently, it has been suggested that on increasing the tendency to homo-coordination an highly nonlinear behavior of the critical demixing density versus the matrix density should be expected [6]; however, these authors were prevented to verify it accurately because simulation at conditions of high nonadditivity is a time-consuming procedure. Calculations in order to estabilish this possibility within our approach are currently in progress.

ACKNOWLEDGMENTS

G.P. was supported by a grant of Consiglio Nazionale delle Ricerche (CNR) and of Fondazione "Angelo Della Riccia." He warmly thanks Dr. Lee's research group for the kind hospitality and helpful discussions during his stay in Norman at the School of Chemical Engineering and Materials Science of the University of Oklahoma (USA). D.S.W. and L.L.L. were supported by the National Science Foundation (Grant Nos. CTS 0114123 and CISE/EIA 0203481) of and the Oklahoma Nanonet. They gratefully acknowledge this support.

[1] B. J. Frisken, F. Ferri, and D. S. Cannell, Phys. Rev. Lett. **66**, 2754 (1991).
[2] D. Nicholson, and K. E. Gubbins, J. Chem. Phys. **104**, 8126 (1996).
[3] L. D. Gelb, K. E. Gubbins, R. Radhakrishnan, and M. Sliwinska-Batkowiak, Rep. Prog. Phys. **62**, 1573 (1999).
[4] O. Barbieri, F. Eheburger-Dolle, T. P. Rieker, G. M. Pajonk, N. Pinto, and A. V. Rao, J. Non-Cryst. Solids **285**, 109 (2001).
[5] M. C. Goh, W. I. Goldburg, and C. M. Knobler, Phys. Rev. Lett. **58**, 1008 (1987); M. Alvarez, D. Levesque, and J. J. Weis, Phys. Rev. E **60**, 5495 (1999).
[6] O. Sierra and Y. Duda, Phys. Lett. A **280**, 146 (2001); E. Scholl-Paschinger, D. Levesque, J. J. Weis, and G. Kahl, Phys. Rev. E **64**, 011502 (2001).

[7] W. Madden and E. D. Glandt, J. Stat. Phys. **51**, 537 (1988); J. Given and G. Stell, J. Chem. Phys. **97**, 4573 (1992); E. Paschinger and G. Kahl, Phys. Rev. E **61**, 5330 (2000).
[8] L. L. Lee, J. Chem. Phys. **103**, 9338 (1995).
[9] M. J. Fernaud, E. Lomba, and L. L. Lee, J. Chem. Phys. **111**, 10 275 (1999).
[10] L. L. Lee and A. Malijevsky, J. Chem. Phys. **114**, 1 (2001).
[11] E. Lomba, M. Alvarez, L. L. Lee, and N. G. Almarza, J. Chem. Phys. **104**, 4180 (1996).
[12] E. Lomba and L. L. Lee, Int. J. Thermophys. **17**, 663 (1996); L. L. Lee, D. M. Ghonasgi, and E. Lomba, J. Chem. Phys. **104**, 8058 (1996); L. L. Lee, *ibid.* **107**, 7360 (1997).
[13] Y. Duda, L. L. Lee, Y. Kalyuzhnyi, W. G. Chapman, and P. D. Ting, J. Chem. Phys. **114**, 8484 (2001); Y. Duda, L. L. Lee, Y. Kalyuzhnyi, W. G. Chapman, and P. D. Ting, Chem. Phys. Lett. **339**, 89 (2001).
[14] See, e.g., E. Meeron and A. J. F. Siegert, J. Chem. Phys. **48**, 3139 (1968); L. Lee and Shing, *ibid.* **91**, 477 (1989).
[15] C. Caccamo, Phys. Rep. **274**, 1 (1996); C. Caccamo and G. Pellicane, J. Chem. Phys. **117**, 5072 (2002).
[16] See, e.g., L. L. Lee, *Molecular Thermodynamics for Nonideal Fluids* (Butterworth, Boston, 1988), pp. 216–218.
[17] L. Verlet, Mol. Phys. **41**, 183 (1980).
[18] J. K. Percus and G. J. Yevick, Phys. Rev. **110**, 1 (1958).
[19] G. A. Martynov and G. N. Sarkisov, Mol. Phys. **49**, 1495 (1983).
[20] See, e.g., M. P. Allen and D. J. Tildesley, *Computer Simulation of Liquids* (Clarendon, Oxford, 1987).
[21] D. J. Adams, Mol. Phys. **29**, 311 (1975).
[22] M. Mezei, Mol. Phys. **40**, 901 (1980); **61**, 565 (1987).
[23] J. D. Weeks, D. Chandler, and H. C. Andersen, J. Chem. Phys. **54**, 5237 (1971).
[24] L. L. Lee J. Chem. Phys. **97**, 8606 (1992).
[25] E. Kieklik, M. Rosinberg, G. Tarjus, and P. A. Monson, J. Chem. Phys. **110**, 689 (1999).
[26] D. Gazzillo, J. Chem. Phys. **95**, 4565 (1991).